Increasing the Structural Chirality of Metal Nanocrystals Created by Circularly Polarized Light via Surface Ligand Engineering

*Tian Qiao, Priyanuj Bordoloi, Anne E. Ashworth, Tsumugi Miyashita, Seyedeh Shadi Mirmohammadi, Jennifer A. Dionne, * and Ming Lee Tang**

T. Qiao, A. Ashworth, S. Mirmohammadi, M. Tang
Department of Chemistry,
University of Utah,
Salt Lake City, UT 84112,
United States,
E-mail: minglee.tang@utah.edu

P. Bordoloi, J. Dionne
Department of Materials Science and Engineering,
Stanford University,
Stanford, CA 94305,
United States,
E-mail: jdionne@stanford.edu

T. Miyashita
Department of Biomedical Engineering,
University of Utah,
Salt Lake City, UT 84112,
United States.

Funding: Air Force Office of Scientific Research under AFOSR Award No. FA9550-23-1-0146, FA9550-20-1-0112. National Science Foundation (CHE-2147792). DARPA grant under the SCOPE program.

Keywords: chiral metal nanostructures, plasmon-mediated synthesis, circularly polarized light, surface ligands

Plasmon-mediated synthesis enables isotropic metal nanocrystal growth with linearly polarized light. This limited dependence on the polarization of incident light during synthesis restricts the structural chirality of nanocrystals produced with circularly polarized light (CPL). Our study here demonstrates that surface engineering of initial achiral silver nanorods (AgNRs) can enhance the structural chirality of the resulting nanostructures produced with CPL. Specifically, the surface ligand hexadecyltrimethylammonium bromide (CTAB) stabilizes the lateral (100) facet-terminated sides of achiral AgNRs and inhibits lateral growth. This surface engineering with achiral ligands results in increased dissymmetry of the nanostructures during the early stages of photo-growth and leads to the formation of "hook" structures, where silver preferentially deposits near the tips of the nanorods. Upon further CPL illumination, these "hook" structures exhibit a significantly larger dissymmetry in the local electric field enhancement distribution compared to the initial achiral AgNRs. This highly dissymmetric electric field enhancement profile influences subsequent growth, resulting in AgNRs with enhanced structural chirality. Notably, the optical dissymmetry of these chiral nanostructures with *g-factor* ~0.05 is an order of magnitude greater than that reported in previous studies conducted under similar chemical conditions but without surface engineering.

1. Introduction

Homochirality is considered a signature of life.[1, 2] Circular dichroism (CD) and optical rotatory dispersion (ORD) are common tools for analyzing materials to quantify their optical dissymmetry, purity, and enantioselectivity. The size mismatch between small molecules and light means molecular chiroptical signatures are very small.[3] In contrast, chiral plasmonic nanocrystals (NCs) have emerged as promising platforms for the ultrasensitive detection of asymmetric small molecules due to their strong interaction with light.[4-6] Moreover, plasmonic NCs can also be used to conduct enantioselective synthesis.[7] While nature can easily encode the handedness of small biomolecules, studying and imparting chirality in macromolecules and inorganic materials, such as plasmonic nanocrystals, is a challenge.

The fabrication of chiral plasmonic NCs requires a symmetry-breaking agent.[8] Early studies used a chiral molecular precursor to assemble achiral NCs.[9-12] Recent breakthroughs using amino acids, peptides[13] and micelles[14] enable chiral metal NCs with distinct morphologies.[15-20] Circularly polarized light (CPL) has also been used as a symmetry-

breaking reagent for NC synthesis.[21-29] CPL possesses several advantages: it is traceless and it can be potentially combined with laser-based nanofabrication technologies for wafer-scale device fabrication.[30] CPL was first used to synthesize chiral semiconductor NCs over a decade ago.[22, 23] Recently, Saito et al. have shown that a chiral gold nanorod (AuNR)/PbO_2 metal-semiconductor heterostructure can be fabricated by depositing PbO_2 preferentially at the optical hot spots of AuNRs under CPL irradiation.[25, 26] The deposition of PbO_2 occurs at regions of the strongest electric field. The distribution profile of the electric field enhancement is chiral owing to the incident CPL, resulting in structural chirality.[31, 32] The excitation wavelength is also important in determining the structural chirality and optical activity of chiral Au bipyramid (AuBP)/PbO_2 nanostructures.[27] We found that the optical activity of Au/PbO_2 heterostructures is dictated by the perturbation introduced by PbO_2 on the dielectric constant in the near-field of the AuBP.

Beyond semiconductor NCs and metal-semiconductor nanostructures, plasmon-mediated synthesis can produce fully metallic NCs with light. This is an important branch of metal NC synthesis.[33-46] When metal NCs are excited, hot electrons have been shown to reduce $Ag^+$and $AuCl_4^-$ in the presence of hole scavengers. Recently, NCs showing optical activity with CPL as the symmetry-breaking agent were demonstrated.[24, 28, 29] Despite the encouraging circular dichroism spectra, electron microscopy of these NCs did not show clear structural handedness. This implied that CPL alone did not create a large dissymmetry in the hot electron density profile, and hence, spatially selective metal photodeposition was limited. Furthermore, earlier studies have suggested a very weak dependence of the metal NC growth on incident light polarization.[39, 42] For example, Redmond et al. reported isotropic Ag growth on immobilized spherical Ag seeds under linearly polarized light.[39] Understanding this weak polarization dependence is important in achieving greater structural chirality and stronger optical activity of metal nanostructures.

Plasmon-mediated synthesis of metal NCs is hot electron driven. The weak polarization dependence can be attributed to a low spatial dissymmetry of the hot electron distribution profile. This hot electron distribution is closely related to electromagnetic field enhancement, which is dictated by the shape of the NC, and the energy and polarization of the incoming beam.[31] Still, it can be very complicated when considering the energetic and temporal evolution of electron at interfaces.[47-54] When the reactions are energetically demanding, only high-energy hot electron or holes are useful, and the reaction yield spatially aligns with the

electromagnetic field distribution. [49-52, 55] This scenario includes the photooxidation of Pb^{2+} to deposit PbO_2. However, hot electrons are dynamic and can diffuse away from the optical hot spot and cool down to become "warm electrons." Photochemical reactions catalyzed by "warm electrons" are not localized by field enhancement. Chemical conditions, e.g., pH and surface passivation, can further modify their spatial distribution. An example is the plasmon-mediated synthesis of Au NCs, where the surfactant polyvinylpyrrolidone (PVP) relays hot electrons to reduce $AuCl_4^-$, dictating the final NC structure.[42] Ag (I) and Au (III) reduction potentials suggest their reduction is not energetically demanding. ($AgCl/Ag$: 0.80 V vs. SHE and $AuCl_4^-/Au$: 0.99 V vs. SHE).[56] Hence, they can be accessed by "warm electrons" far from the hot spots. For the polarization of light to dictate the spatial distribution of non-energy demanding reactions on the NC surface, the dissymmetry of the hot electron-mediated reaction spatial distribution must be enhanced. This can be achieved by biasing the reaction location with chemical conditions or amplifying dissymmetry in the electromagnetic field distribution with anisotropic particles.

Here, we report the fabrication of chiral AgNRs with well-defined structural chirality using CPL. We engineer the spatial dissymmetry of Ag^+ reduction by chemically passivating the surface of the achiral NRs. We control the surface density of CTAB, the achiral ligand on the AgNRs, to direct Ag growth on the tips of the nanorod at early stages. AgNRs with plasmon-mediated Ag tip deposits seed subsequent Ag growth based on an enhanced dissymmetry of the electric field enhancement distribution courtesy of particle anisotropy. The polarization-dependent field distribution dominates the subsequent growth of the NCs, generating NCs with well-defined structural chirality. The optical dissymmetry factor (*g-factor*) of our chiral AgNRs is an order of magnitude larger than chiral Ag nanostructures obtained with similar reaction conditions,[29] resulting from the improved structural chirality. The *g-factor* we obtain is more than double that of previous studies of chiral AuBP/PbO_2 nanostructures at ~0.02.[27]

2. Results and Discussion

To synthesize all-plasmonic chiral NCs using CPL, we first immobilized our AgNRs from a colloidal solution onto ITO glass substrates. (**Figure 1a**) By fixing the NCs on a substrate, CPL excitation is unidirectional on the nanorod, generating a larger dissymmetry in the electric field enhancement distribution compared to free NCs in solution.[31, 32, 57, 58] These achiral, pentagonal AgNRs served as the seeds for chiral AgNRs. The high-quality precursor

AgNRs were synthesized via AuBP-directed seeded growth developed by Zhuo et al.[59, 60] The AuBPs were synthesized following the report by Sanchez-Iglesias et al.[61] The details can be found in the Experimental Section. The average length of the AgNRs is 223 nm ± 18 nm with a width of 30 nm ± 2 nm and an aspect ratio of ~7.4. The extinction spectrum of AgNRs demonstrates a longitudinal localized surface plasmon resonance (L-LSPR) at ~1230 nm, a transversal LSPR (T-LSPR) at ~ 400 nm, and higher order L-LSPR at ~680 nm and ~550 nm. (**Figure 1b**) The transmission electron microscopy (TEM) images of the achiral AuBPs and AgNRs are presented in **Figure S1**. Previous studies have shown that the contribution of the AuBP core to the optical properties of the AuBP@AgNR NC is negligible.[60] Therefore, we will use AgNRs to denote our NCs throughout the paper for simplification.

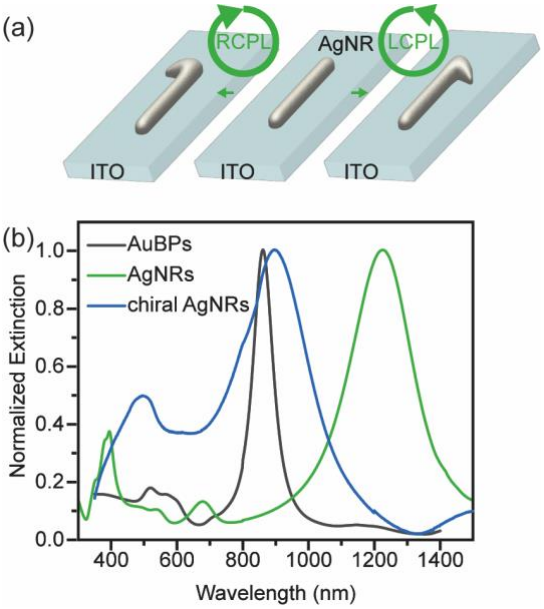

Figure 1. (a) Schematic of the plasmon-mediated growth of chiral AgNRs from achiral NCs using CPL. (b) Normalized extinction spectra of AuBPs and AgNRs in water and chiral AgNRs on ITO glass after 60 min 200 mW cm^{-2} 532 nm LCPL.

To synthesize chiral AgNRs with CPL, we conducted the plasmon-mediated synthesis by immersing the ITO/AgNRs substrate in a cuvette containing 1 mM $AgNO_3$ and 1 mM sodium citrate. Citrate, the hole scavenger,[33] was oxidized to CO_2 and 1,3-acetonedicarboxylate following **Equation 1**.[37, 38, 44] We illuminated the substrate with 200 mW cm^{-2} 532 nm CPL from the back side of the ITO glass. Since ITO has a high work function, its impact on the photochemical reactions here is negligible.[62] It is important to point out that we conducted all photochemical reactions oxygen-free, with the solutions prepared in a glovebox and the cuvettes sealed. When the reaction was conducted in the air, very complex NC morphologies

without clear structural chirality were obtained. (**Figure S2b**). In the presence of O_2, many NCs nucleated independently from the AgNRs on the substrate. The CD of these samples exposed to oxygen had low signals compared to oxygen-free synthesis. (**Figure S2a**) Early studies on plasmon-mediated synthesis outlined the photo-oxidative etching of Ag following **Equations 2 and 3**.[40, 44] This highly efficient reaction provides Ag^+ for the growth of triangular nanoprisms. In our experiments, we suspect this process complicated the growth pathway toward chiral AgNRs. We postulate that oxygen is easily reduced by the hot electrons from the AgNR, providing hydroxide ions that accelerate the citrate oxidation, creating long-lived electrons that diffuse over the ITO, which then reduce silver ions to metallic silver. In our synthesis, eliminating oxygen led to better control of the distribution of hot electrons for photochemistry.

$$C(OH)(COO^-)(CH_2COO^-)_2 + OH^- \rightarrow CO(CH_2COO^-)_2 + CO_2 + H_2O + 2e^- \quad (1)$$

$$Ag^+ + e^- \rightarrow Ag \quad (2)$$

$$O_2 + 2H_2O + 4e^- \rightarrow 4OH^- \quad (3)$$

To understand how the well-defined structural chirality of the AgNRs developed, we tracked the evolution of the particle morphology. We utilized the Gaussian profile of the laser beam to identify AgNRs at different growth stages. The achiral AgNRs located at the center of the beam received more photons than the ones at the edge and are thus at a more advanced stage of growth. The distance from the center of the laser beam is inversely proportional to the amount of silver deposited. As shown in **Figure 2a**, under the illumination of 532 nm left circularly polarized light (LCPL), Ag growth first occurred at one end of the AgNRs. Then, subsequent growth was guided by this initial tip deposition, forming a hook on one end of the AgNR. As more silver was deposited, the hook developed a helical twist and propagated along the length of the nanorod. Eventually, silver grew on the opposite tip of the AgNRs, creating an overhang. Similar observations were made with right circularly polarized light (RCPL) as the chiral directing agent, with the final optically active structure also evolving from an initial deposit on one tip of the AgNRs. (**Figure 2b**) At each stage, the structures obtained under LCPL and RCPL exhibit opposite handedness. Broader view images showing a few of the final chiral structures are shown in **Figure 2d** and **2e**.

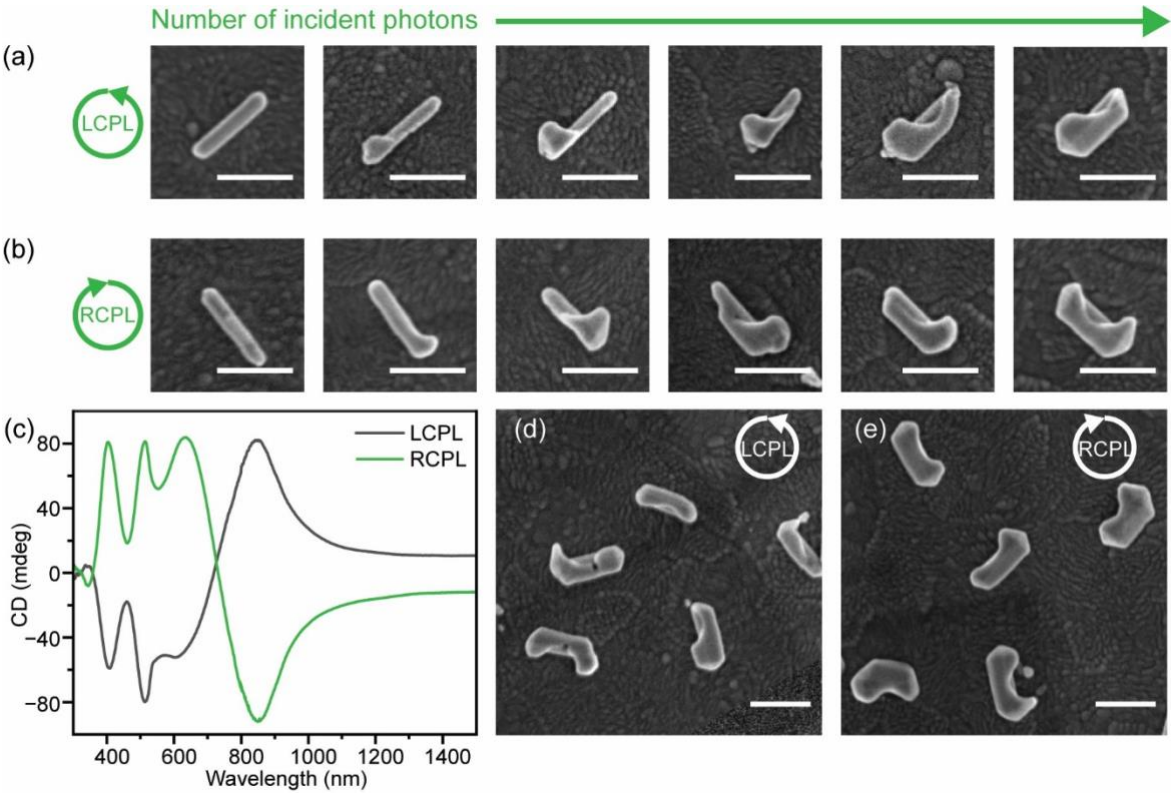

Figure 2. Structural evolution of chiral AgNRs enabled by 532 nm CPL. (a) SEM images of the structural evolution of chiral AgNRs under a 532 nm (a) LCPL and (b) RCPL excitation. (c) Ensemble CD spectra of AgNRs after 60 min of 532 nm CPL illumination. SEM images showing the morphology of chiral AgNRs after 60 min of 532 nm (d) LCPL and (e) RCPL illumination. All scale bars are 200 nm.

Figure S3 has additional broad-view SEM images of chiral AgNRs at different growth stages, showing that most AgNRs follow the growth process presented in **Figure 2**. We cannot unambiguously assign a handedness to 50~60% of the NCs at the final stage. For the ones showing clear dissymmetry, the proportion of one-handedness is double the other. (**Table S1**) Ensemble CD spectra of the chiral AgNRs are shown in **Figure 2c**, illustrating the chiroptical properties of these NCs. Some structural inhomogeneity is visible in these images, with chiral AgNRs in the same view in different growth stages, showing slight variations in the shape and size of new Ag deposits. Several factors contribute to this structural inhomogeneity. The first one is the inhomogeneity in the morphology of the achiral AgNR precursors, which can cause small variations in individual NC's light-matter interactions. Second, the rough ITO surface can lead to variation in AgNR adhesion to the substrate and orientation relative to the incident light. The surface chemistry of the NCs can also affect the final structures of NCs, discussed in detail below. These three sources of inhomogeneity may also lead to preferential Ag

growth on one tip rather than both. **Table S2** and **Figure S4** further show that the preferential growth on one tip of the achiral AgNRs is independent of the achiral AgNR aspect ratio or the polarization of the light. Similar observations were made on chiral AuBP/PbO_2 nanostructures, where many AuBPs had PbO_2 deposited on one side at the early growth stage but subsequently evolved to have PbO_2 deposited opposite the initial site.[27]

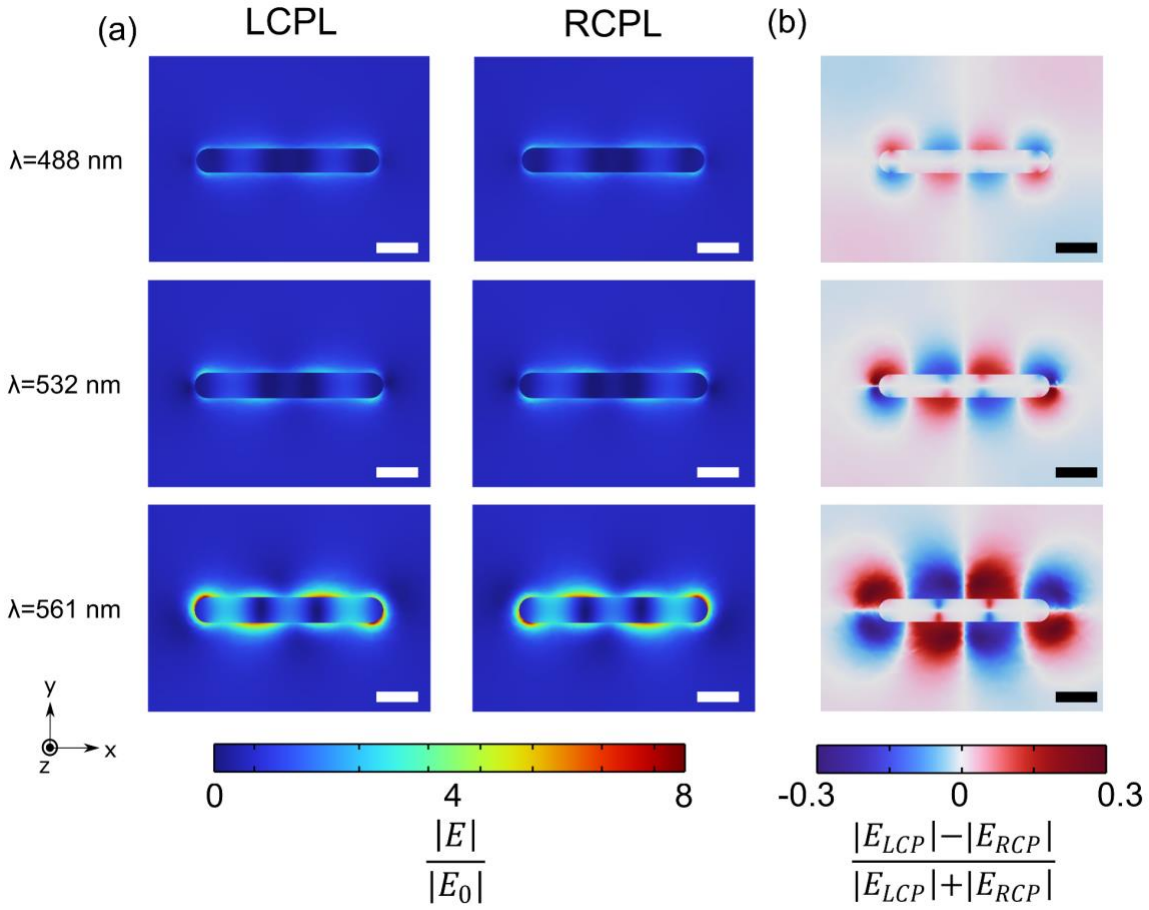

Figure 3. Longitudinal electric field enhancement profile for 488, 532, and 561 nm excitation. (a) LCPL illumination and RCPL illumination (along z-axis) on the achiral AgNRs. (b) Normalized differences in electric field amplitude distributions for LCPL and RCPL illumination at 488, 532, and 561 nm incident wavelength (from top to bottom); AgNR dimensions: Length ~ 223 nm, Width ~ 30 nm. Scale bars: 50 nm.

The structural evolution of the chiral AgNRs in **Figure 2** is unexpected according to the electric field distribution at these excitation wavelengths, as explained below. Using a FEM solver (COMSOL), we simulated an AgNR in an aqueous medium similar to that of the experimental conditions to understand the electric field enhancement distribution under CPL

illumination. **Figure S5** displays the numerically calculated extinction spectra of AgNR, which clearly shows that the excitation wavelengths are near the higher order LSPR, which is spectrally separate from the Ag plasmonic resonance. This is important since the excitation wavelength is spectrally near the higher-order LSPR, resulting in the electric field distribution observed in **Figure 3**. To better understand the enhanced electric field's spatial distribution on the AgNR, we also plot the electric field enhancement on an arc starting from one tip to the other through the top surface of the AgNR in **Figure S6**. We observe that electric field enhancement is distributed over the tips and the waist for all excitation wavelengths, with the distribution moving preferentially towards the tips for longer excitation wavelengths. The electric field enhancement distribution shows the characteristic chiral distribution of hotspots, resulting from interference of the T-LSPR and L-LSPR modes that can be excited by CPL illumination.[31, 63, 64] Further, the electric field amplitude profile dissymmetry, which is the normalized difference in electric field amplitude distributions for LCPL and RCPL illumination is given in **Figure 3b**. Normalization helps us compare the spatial distribution across all illumination wavelengths and restricts the values between -1 and 1. This provides a visual tool to observe the difference between the spatial distribution of the electric field amplitude during CPL illumination and comment on the chirality of the electric field amplitude profile only. This also allows us to locate the regions primed for hook growth on the AgNR according to CPL illumination, e.g., photoreduction at the top-right tip area of the AgNR is favored during RCPL illumination, which is clearly observed experimentally in **Figure 2b.**

We can clearly observe that there are electric field hotspots on the waist, too, but we do not observe substantial growth in these regions until the tip growth spreads to these areas, as observed in **Figure 2a, b**. That is, if the photochemical reduction is solely dictated by electric field enhancement distribution, Ag growth is expected to grow on the sides and tips of the achiral AgNRs simultaneously. Furthermore, the electric field distribution suggests equal Ag deposition on both sides of the achiral AgNRs. This contrasts with the experimental observation of hook structure formation initially, indicating that CPL alone cannot cause preferential Ag deposition at one tip.

The discrepancy between the observed experimental results from simulations suggests Ag growth on both lateral sides of the achiral AgNRs was suppressed. This observation inspired us to explore the chemical origin of the spatial distribution of Ag deposition dictating the final

chiral structure. During the growth of the AgNRs, hexadecyltrimethylammonium chloride (CTAC) was employed. The as-synthesized AgNRs were precipitated by centrifugation and purified by depletion interaction-induced self-separation in a concentrated hexadecyltrimethylammonium bromide (CTAB) solution (50 mM).[59] The ligands of the AgNRs are thus primarily CTAB with a small amount of CTAC; both bind to the surface of AgNRs in a similar manner.[65] Previous studies illustrated that the achiral AgNRs retain the pentagonal symmetry from the AuBPs.[66, 67] These AgNRs consist of 5 (100) lateral facets and 10 (111) facets at the tips.[68] A detailed mechanistic study has shown that halide stabilizes the (100) facets and leads to preferential growth on the (111) tip facets. This limits growth along the short transversal axis and encourages growth along the ends of the AuBPs, resulting in the NR morphology.[69] When we conducted the plasmon-mediated synthesis on these achiral NR seeds, this ligand-directed growth likely dominated the early stage, resulting in preferential Ag deposition at the tips.

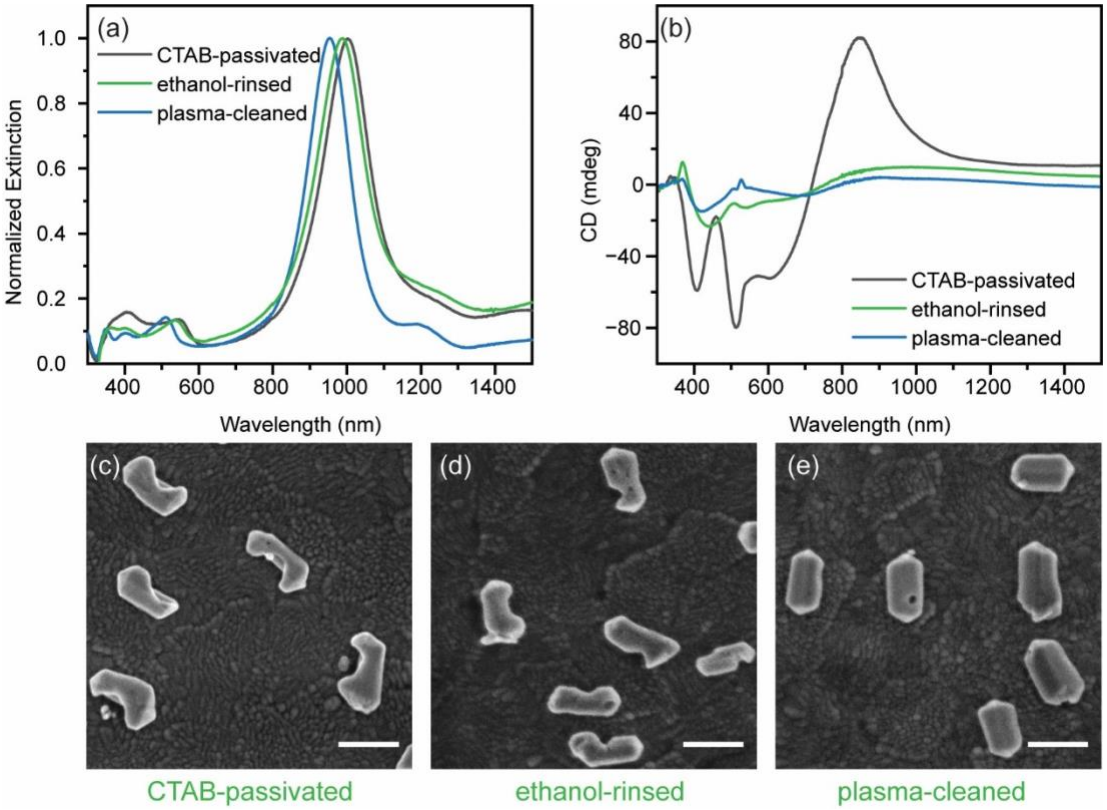

Figure 4. The effect of NC surface passivation on AgNRs structural chirality. (a) Normalized extinction spectra showing the blue shift of the CTAB passivated achiral AgNRs (adsorbed on substrate) LSPR (black) after ethanol rinse (green) or plasma cleaning (blue). (b) The corresponding CD spectra of chiral AgNRs synthesized from CTAB passivated (black), ethanol rinsed (green), and plasma-cleaned achiral AgNRs (blue). Morphology of chiral

AgNRs developed from (c) CTAB passivated-, (d) ethanol rinsed- and (e) plasma cleaned-achiral AgNRs. All scale bars are 200 nm.

To test our hypothesis, we removed the surface ligands from the achiral AgNRs and tracked their structural evolution under 532 nm LCPL irradiation for 60 minutes. The removal of the surface ligands by ethanol rinsing and plasma cleaning was corroborated by the blue shift of the LSPR of the NRs, as in **Figure 4a**, due to the smaller refractive index surrounding the AgNRs when exposed to air. The ethanol-rinsed NR seeds grew into NCs with decreased structural chirality (**Figure 4d**), as reflected in the significantly compromised CD (**Figure 4b**), where the maximum CD intensity compared to the CTAB-coated precursors decreased by ~75%. Plasma-cleaned achiral NRs[70, 71] resulted in nanostructures with little to no CD, as shown in **Figure 4e**. The CD intensity of this sample is even lower than the ethanol-rinsed one, consistent with the symmetric pentagons shown in SEM. Broad-view SEM images in **Figure S7** demonstrated that the Ag was deposited on the lateral sides even at the early growth stage of the surface-cleaned seeds. Without CTAB, silver deposition was initially distributed relatively uniformly on the nanocrystal surface. Over time, this uniform growth persisted, and the AgNRs grew in their width. Consequently, low CD intensity was observed in these nanostructures due to their low structural dissymmetry. This shows that the reduced structural chirality of the NCs after 60 min of CPL illumination is not due to faster Ag growth but to diminished spatial selectivity of Ag growth on the surface-cleaned seeds. The “hook” structure formation is also absent in the early stage due to removal of the CTAB surface ligand.

Although lateral Ag growth was observed, the relatively isotropic Ag deposition of the ligand-free achiral AgNRs does not fully align with the simulations in **Figure 3**; however, it is more consistent with the weak polarization dependence of the plasmon-mediated Ag growth in earlier studies.[39] Additionally, the photothermal effect could facilitate the isotropic Ag deposition on NRs.[72] Although the interband transition threshold in Ag has been reported to be > 3 eV,[73] which is beyond the highest energy of excitation used in this study (2.5 eV), hot electrons generated by interband transitions that lead to isotropic Ag deposition[74] cannot be ruled out without detailed simulation of the hot carrier generation rate of AgNRs. A molecular-level mechanistic study on the plasmon-mediated synthesis of Ag nanocrystals in the future could enhance our understanding of how the energetics and temporal evolution of hot electrons and nanocrystal surface temperature influence nanoparticle growth patterns.

Nonetheless, the significance of surface ligand passivation in enhancing the spatial selectivity of plasmon-mediated chemical reactions is demonstrated.

Previous studies also observed the significant impact of ligand passivation on plasmonic NC surface chemistry. For example, Al-Zubeidi et al. have shown that Au facets can be selectively dissolved depending on surface passivation.[75] They observed isotropic dissolution of Au by halide on AuNRs cleaned by plasma. Conversely, AuNRs with the original CTAB bilayer showed preferential dissolution from the tips, where CTAB packing density was lower. The plasmon-mediated synthesis of Au NCs also showed the key role of PVP in dictating the NC growth pattern[42] where the Au only grew on the PVP passivated sites.

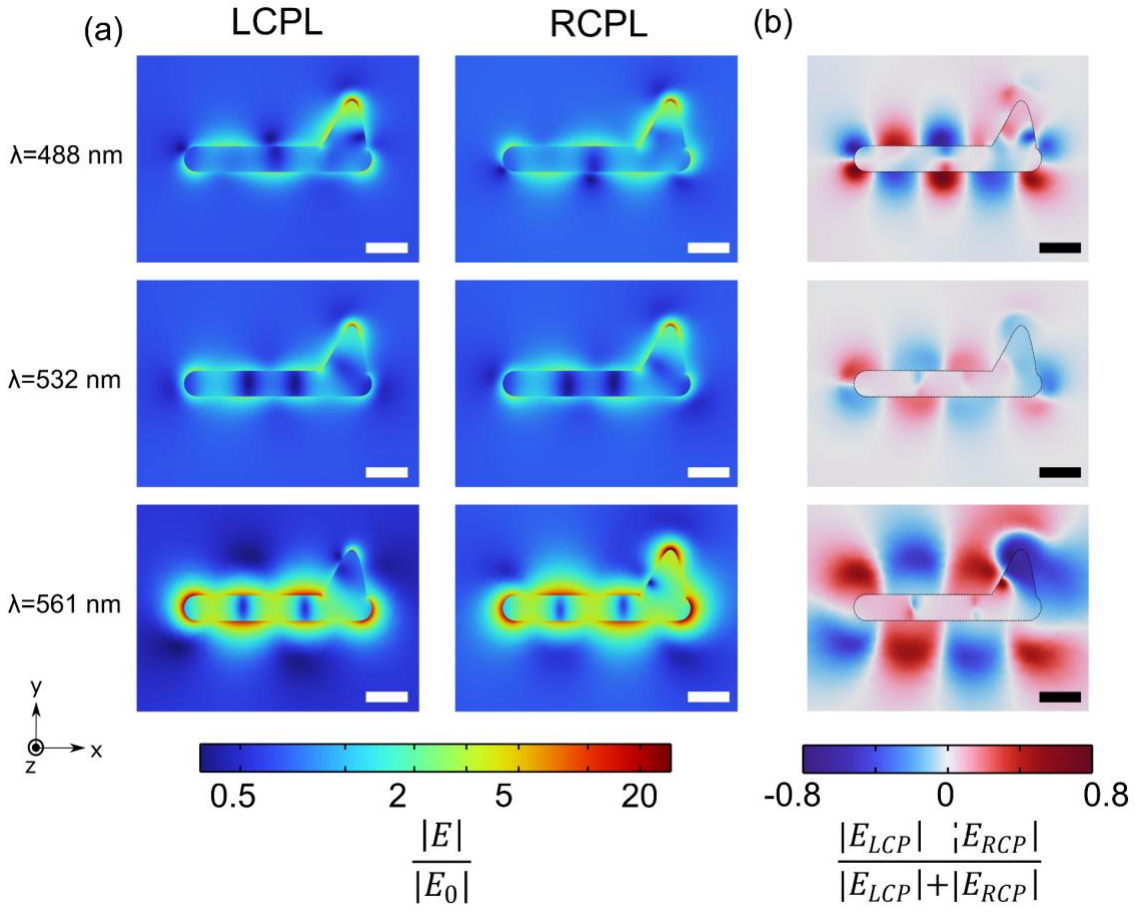

Figure 5. Longitudinal electric field enhancement profile for 488, 532, and 561 nm excitation. (a) LCPL illumination and RCPL illumination (along z-axis) on the hooked AgNRs. (b) Normalized differences in electric field amplitude distributions for LCPL and RCPL illumination at 488, 532, and 561 nm incident wavelength (from top to bottom); AgNR dimensions: Length ~ 223 nm, Width ~ 30 nm, Hook height ~ 50 nm. Scale bars: 50 nm.

We further simulated tip-deposited AgNRs designed to represent a typical hook structure generated under RCPL, as shown in **Figure 5**. Our results indicated a substantial enhancement of the local electric field enhancement (i.e., 20x of the incident electric field amplitude) at the hooks. This suggests that once the hooks appear due to the ligand-directed deposition, the electric field amplitude plays a more dominant role in Ag growth, and subsequent illumination increases the hook growth, as observed in **Figure 2.** Another interesting observation is that large electric field enhancement at the hook is observed for both LCPL and RCPL illumination, even though the location of the initial growth is preferential to one type of CPL illumination. Moreover, the electric field amplitude also turns out to be the largest at the tips and not the waist, which results in more Ag growth on the existing hook. **Figure S8** shows the calculated extinction spectra of this structure, clearly showing the influence of the hooks with the introduction of sharp extinction spectra peaks in 400 nm – 800 nm wavelength, which could be a cause of the broad bandwidth in the experimental extinction spectra in the same wavelength range. Simulations also show these four peaks have an asymmetric response to CPL illumination, which results in slightly perturbed extinction spectra (refer to **Figure S8 a, b**) and large CD values, consistent with the experimental observations.

From the discussions above, we can conclude that the hot electron distribution that dictates chiral AgNR growth is regulated by two parameters: polarization-dependent field distribution and surface chemistry. The surface passivation by CTAB facilitates the early dissymmetric NC growth. We hypothesize that the denser halide packing on (100) facets, compared to (111) facets, makes Ag deposition sites more available on (111) facets. [69]Since the achiral AgNR tips are enclosed by (111) facets, the deposition of Ag through Ag^+ reduction by hot electrons is preferred near the tips of the achiral AgNRs. The dissymmetry of hot electron-mediated Ag deposition spatial distribution is thus enhanced by CTAB binding to the NR surface during the early stage of CPL illumination, generating the hook structure. The early dissymmetric "hook" structures are critical in seeding the later growth stage because they provide enhanced dissymmetry of the hot electron distribution. This enhancement occurs because the shape of the nanocrystal, the polarization, and the energy of the incoming beam dictate the spatial distribution of the local electric field enhancement.[76] Consequently, the spatial dissymmetry of the hot electron distribution improves with increasing nanocrystal shape dissymmetry during the growth process in the presence of CTAB. This is seen by comparing the simulation results in **Figure 3** and **Figure 5**, where the formation of "hook" structures results in a higher

maximum enhancement of incident beam electric field amplitude (20x vs. 8x) and a larger contrast between LCPL and RCPL illumination (0.8 vs. 0.3). We note that because the temperature on the plasmonic NC is typically spatially uniform, photothermal effects are likely not the primary reason for dissymmetric growth.[77, 78]

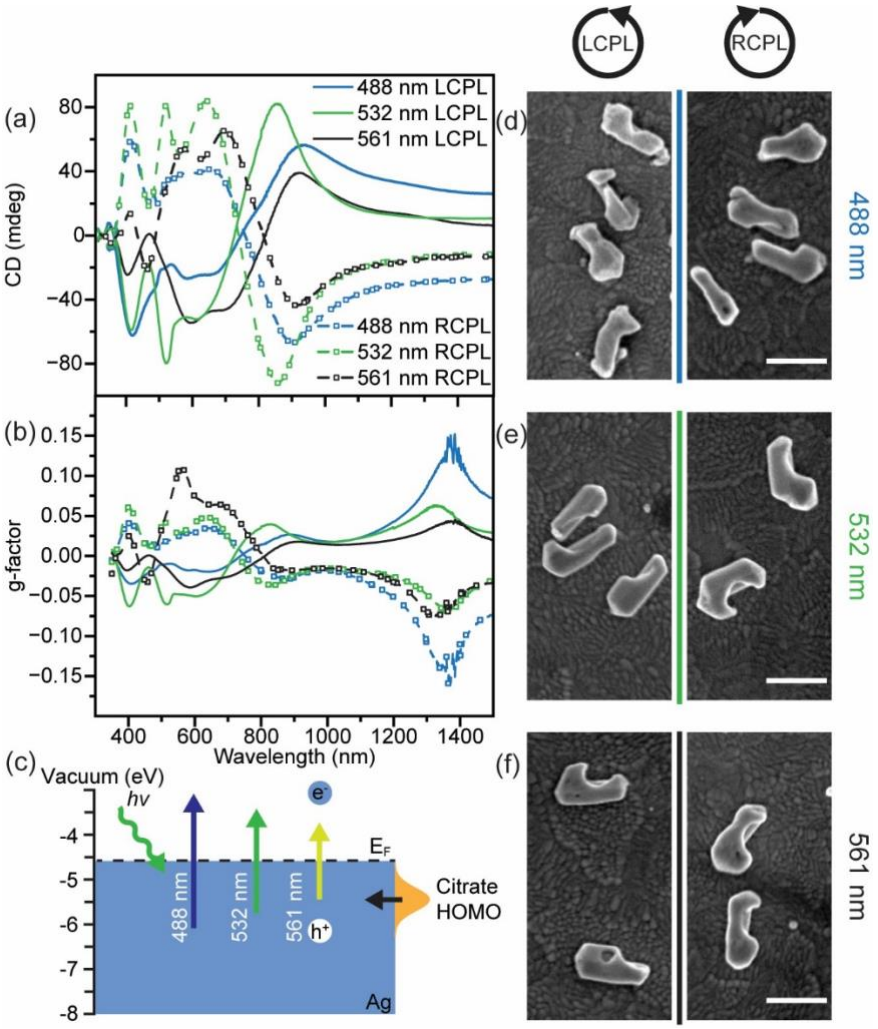

Figure 6. Effect of CPL excitation wavelength on the optical and structural chirality of AgNRs. (a) CD and (b) *g-factor* spectra of chiral AgNRs synthesized by illumination with 488 nm, 532 nm and 561 nm CPL. (c) Energy diagram depicting the possible mechanism of plasmon-mediated synthesis by citrate oxidation. SEM images of the chiral AgNRs synthesized with (d) 488, (e) 532 and (f) 561 nm CPL. All scale bars are 200 nm.

We further examined the impact of the excitation wavelength on the chiral structures. We illuminated the achiral AgNRs with 488 and 561 nm CPL at the same photon irradiance and compared them to 532 nm CPL. The detailed excitation conditions are in **Table S3**. The chiral

morphologies obtained are similar, with 488 nm CPL leading to slightly more irregularities. The broad-view SEM images of these chiral AgNRs can be found in **Figure S9**. The small variations of their CD spectra suggest different structural chirality but might be challenging to resolve using SEM. The relationship between optical activity and excitation wavelength highlights the importance of the electric field enhancement distribution in growth patterns. This significance could be considerably diminished without CTAB passivation.

We calculated Kuhn's dissymmetry factor (*g-factor*) of the chiral AgNRs using **Equation 4** and the extinction spectra shown in **Figure S10**. (**Figure 6b**) At ~1400 nm, a *g-factor* > 0.1 was obtained for chiral AgNRs grown under 488 nm CPL. However, the *g-factor* at this wavelength is not practically meaningful as the chiral AgNRs interact with light very weakly. At ~ 800 nm where the chiral AgNRs interact with light strongly, *g-factor* ~ 0.05 was obtained. This number is double the *g-factor* of the AuBP/PbO_2 nanostructures, benefiting from the all-plasmonic nanostructures here. The *g-factor* of our chiral AgNRs is an order of magnitude bigger than that reported in reference 29, where similar reaction conditions were employed. We noticed that no ligand participated in the reaction in reference 29, and relatively weak structural chirality was observed. A table comparing the *g-factor* and synthetic conditions of chiral nanostructures in this study and in reference 29, along with relevant previous studies,[24, 28, 57, 58] can be found in the Supporting Information **Table S4**. Our simulations also show higher *g-factor* values as large as ~ 0.5 near the wavelengths of the four extinction cross-section peaks, (**Figure S11**) as expected from the large CD values, even though the experiment did not observe such values due to the AgNR ensemble effect explained in the AgNR simulations part of the Experimental Section.

$$g - factor = 2 \times \frac{CD}{32980 \times Extinction} \quad (4)$$

3. Conclusion

In conclusion, we have shown that surface passivation of achiral metal nanostructures is essential for creating structural chirality with CPL. Without surface passivation, we observed isotropic growth of Ag, resulting in achiral AgNRs. However, when CTAB was used to passivate the achiral seeds, the spatial selectivity of Ag deposition improved, leading to the formation of chiral "hook" structures during the early growth stage. The emergence of these "hook" structures facilitated subsequent nanocrystal growth, which was dominated by an

enhanced dissymmetry in the local electric field enhancement distribution compared to that of the initial achiral AgNRs. Our results provide valuable insight into the synthesis of chiral metal nanostructures using CPL. This will expand the library of available chiral nanostructures and enable the production of nanostructures with improved structural chirality and optical activity. Furthermore, understanding the role of surface passivation in influencing nanocrystal photo growth can be applied in modern nanofabrication technologies to create metal flat optics or heterogeneous catalysts for enantioselective chemical reactions.

4. Experimental Section

Chemicals: Chemical reagents were purchased from Aldrich Chemical Co or MP Biomedicals and were used as received. Ultrapure water (resistivity > 18.2 MΩ cm at 20 °C) was acquired from an Elga water purification system and was used in all experiments.

Instrumentation: Extinction spectra were recorded on a Cary 5000 UV-Vis absorption spectrophotometer. Circular dichroism (CD) spectra were recorded on a Jasco J-1500 CD spectrometer. The 300-800 nm CD spectra were obtained with a Xenon lamp and an EXPM-531 PMT detector. The 800-1600 nm CD spectra were obtained with a Tungsten lamp and an EXIG-542 InGaAs detector. All CD spectra were recorded with 2s D.I.T and 50 nm min^{-1} scan rate with a single scan. CD signal from a circular area with a 4 mm diameter was recorded for all samples. Scanning electron microscopy (SEM) images were obtained on a Helios Nanolab 650 microscope. Transmission electron microscopy (TEM) images were obtained on a JEOL JEM 2800 microscope. A Harrick PDC-32G Basic Plasma Cleaner was used to remove the surfactants on the nanostructures before photodeposition for selected samples.

Notes on linear anisotropy contribution to CD spectra: Samples that exhibit linear anisotropy can generate false CD signals, which may lead to misinterpretation of experimental data when analyzed using commercial CD spectrometers.[79, 80] Research has indicated that the effects of linear dichroism (LD) and linear birefringence (LB) can be averaged out when CD spectra are obtained from four different sample orientations.[81] In this study, the glass/ITO substrates do not produce any CD artifacts, as illustrated in **Figure S12a**. When AgNRs are deposited, they are randomly oriented and do not exhibit ensemble linear anisotropy, as seen in the SEM images in **Figures S3, S7, and S9**. In an extreme case, where seed AgNRs were exposed to 200 mW cm^{-2} of 532 nm linearly polarized light for 60 min to induce linear anisotropy in the film, less than 10 mdeg of CD signals were detected, as shown in **Figure S12b,** which is less than 10%

of CD intensity detected for the chiral AgNRs. This indicated that the possibility of linear anisotropy introducing false CD signals in this study is minimal.

Synthesis of achiral silver nanorods (AgNRs): AuBP nanocrystals were synthesized following methods reported by Sánchez-Iglesias *et al*. [61] All the compounds were mixed in ultrapure water. In a 20 mL scintillation vial placed in an aluminum reaction block, 4 mL of 0.1 M hexadecyltrimethylammonium chloride (CTAC) was brought to 80 °C. 2 mL of 1 mM $HAuCl_4$ and 2 mL of 20 mM citric acid were then added under gentle stirring (200 rpm). While vigorously stirring (1700 rpm), 0.25 mL of 25 mM $NaBH_4$ was freshly prepared with cold water and rapidly injected into the vial. The vial was left uncapped for 2 minutes, then capped, and the seed solution temperature was maintained at 80 °C for 90 minutes with gentle stirring (200 rpm). The final seed solution was stored at room temperature. The growth solution for AuBPs was prepared by combining 40 mL of 0.1 M hexadecyltrimethylammonium bromide (CTAB), 2 mL of 10 mM $HAuCl_4$, 0.4 mL of 10 mM $AgNO_3$, 0.8 mL of 1 M HCl, and 0.32 mL of 0.1 M ascorbic acid in an Erlenmeyer flask in a water bath at 30 °C. Subsequently, 1 mL of seed solution was added to the growth solution to synthesize AuBPs. The mixture was maintained at 30 °C for 3 hours. After centrifugation at 7000 rpm for 20 minutes, the AuBPs were collected as the precipitate and then stored in the refrigerator in the dark.

AgNRs were synthesized based on the methods reported by Zhuo *et al.* [60] with slight modifications. The AuBPs obtained were centrifuged at 7000 rpm for 10 minutes. The precipitate was then redispersed in 30 mL of CTAC (0.08 M) in an Erlenmeyer flask. The flask was heated in a water bath at 60 °C. After that, 6 mL of $AgNO_3$ (10 mM) and 3 mL of ascorbic acid (0.1 M) were added to the flask. The mixture was stirred at 400 rpm for 4 hours to complete the reaction. The product was collected by centrifugation at 7000 rpm for 10 minutes. The precipitate was further purified through re-dispersion in 30 mL of CTAB (0.05 M) overnight.[59] After depletion purification, the AgNRs were dispersed in 1.5 mL of CTAC (1 mM) and stored in a fridge.

Plasmon-mediated growth of chiral AgNRs: The glass substrates coated with indium tin oxide (ITO) were cleaned in a plasma cleaner for 10 seconds at 250 mTorr. Then, 2.7 mL of ethanol was slowly added to 5 mL of AgNRs solution (with extinction of approximately 4 at 350 nm) while stirring. After that, the clean ITO substrates were submerged in the solution for approximately 4 hours to allow the AgNRs to be adsorbed.

Inside a glovebox, the ITO/AgNRs substrates were immersed in an aqueous solution of silver nitrate (1 mM) and sodium citrate (1 mM) in a cuvette. The cuvette was then sealed to avoid the involvement of oxygen in the subsequent reactions. The substrate was illuminated from the backside with LCPL or RCPL for the desired duration. To reduce the CTAB passivation on achiral AgNRs adsorbed on ITO substrates, the substrates were either rinsed ten times with ethanol or cleaned in a plasma cleaner for 40 s (200 mTorr N_2) immediately before photogrowth.

To generate CPL, 488, 532, and 561 nm lasers (OBIS) were passed through Glan laser polarizers (Thorlabs GL10) and quarter waveplates (Newport 10RP54-1B and 10RP54-1). The fast axis of the quarter waveplate was aligned at 45 ° to the polarization plane of the lasers. The handedness of the light was defined from the receivers' point of view following the IUPAC standard.[82] All laser beams were expanded by a set of lenses to at least 4 mm in diameter. The size of the beam was obtained by imaging the beam profile using a CMOS camera (Imaging Source DMK 33UX273) and then fitting the beam profile with Gaussian functions. The irradiance of the lasers can be found in **Table S3**.

AgNR Simulations: COMSOL Multiphysics was used as a FEM solver to understand the electromagnetic response of the Ag nanorod (placed on the ITO glass substrate) to chiral light placed in an aqueous (H_2O) environment. From TEM images, the dimensions of the structure were chosen to represent an ensemble average of AgNR particles with length = 223 nm and width = 30 nm.

The main plasmonic peak undergoes a notable spectral shift due to changes in the dielectric environment of the AgNR, moving from water to air and ITO. Generally, a lower refractive index of the surrounding medium leads to a blueshift of plasmonic peaks. Therefore, transitioning from water ($n_{water} \sim 1.33$) to air ($n_{air} \sim 1$) results in a blueshift, as shown in **Figure 4a**. A similar blueshift occurs when AgNR is positioned on a higher refractive index substrate ($n_{ITO} \sim 2.56$) but exposed in air compared to being dispersed in water. Additionally, in our updated **Figure S5** and **Figure S8**, we observe the expected global redshift of all the plasmonic peaks when immersing ITO/AgNR in a solution due to the addition of a relatively higher refractive index substrate from below it, compared to AgNRs dispersed in water.

AgNR is placed longitudinally on the ITO substrate, and CPL light is illuminated from the bottom. We numerically calculate the extinction cross-section by adding the absorption and scattering cross-section for wavelengths. We observe three sharp resonances at 450 nm, 576

nm and ~1360 nm attributed to the traverse (T-), higher order and longitudinal (L-) localized surface plasmon resonance (LSPR), respectively. The slight mismatch with the experimental spectra compared to the simulation is due to the fact that the former has a large variability in the dimensions of the nanorods, while the latter is an ensemble-averaged result.

We designed a prototypical hooked structure of Ag hook of ~50 nm height on one side of the AgNR. Next, we excite the structures with both CPL illumination and measure the extinction cross-section (σ_ext) to calculate the CD spectrum and Kuhn's dissymmetry factor as shown below:

$$CD = \sigma_{ext,LCPL} - \sigma_{ext,RCPL} \quad (5)$$

$$g - factor = 2 * \frac{\sigma_{ext,LCPL} - \sigma_{ext,RCPL}}{\sigma_{ext,LCPL} + \sigma_{ext,RCPL}} \quad (6)$$

Figure S8 shows the extinction cross-section of the hooked structure (grown under RCPL) for CPL illumination, and we can observe new peaks in the 600 nm – 800 nm CD introduced due to the hook. Moreover, **Figure S11** shows the calculated CD and *g-factor* values are substantially large in the 400 nm-800 nm, similar to the trends observed in the experimental results. We also observe large *g-factor* values for longer wavelengths, as observed experimentally in **Figure 6**. However, AgNRs do not interact with light strongly as there are no plasmonic resonances in these spectral regimes and hence are not practically meaningful. Again, the absence of sharp features in the experimental data is due to an ensemble-average effect.

Acknowledgements

T. Q. and P. B. contributed equally. This material is based upon work supported by the Air Force Office of Scientific Research under AFOSR Award No. FA9550-23-1-0146 for equipment to M.L.T. M.L.T. also acknowledges salary support from the National Science Foundation (CHE-2147792). FA9550-20-1-0112 to MLT. J. D. and P.B. acknowledge funding from a DARPA grant under the SCOPE program.

Conflict of Interest

The authors declare no conflict of interest.

References

(1)Ozturk, S. F., Sasselov, D. D., On the Origins of Life's Homochirality: Inducing Enantiomeric Excess with Spin-Polarized Electrons, 2022, *Proc. Natl. Acad. Sci. U. S. A.,* 119, e2204765119.
(2)Cho, Nam Heon, Guerrero-Martínez, Andrés, Ma, Jessica, Bals, Sara, Kotov, Nicholas A., Liz-Marzán, Luis M., Nam, Ki Tae. Bioinspired Chiral Iorganic Nanomaterials, 2023, *Nat. Rev. Bioeng.,* 1, 88.
(3)Hentschel, M., Schäferling, M., Duan, X. Y., Giessen, H., Liu, N., Chiral Plasmonics, 2017, *Sci. Adv.,* 3, e1602735.
(4)Hendry, E., Carpy, T., Johnston, J., Popland, M., Mikhaylovskiy, R. V., Lapthorn, A. J., Kelly, S. M., Barron, L. D., Gadegaard, N., Kadodwala, M., Ultrasensitive Detection and Characterization of Biomolecules Using Superchiral Fields, 2010, *Nat. Nanotechnol.,* 5, 783.
(5)Warning, L. A., Miandashti, A. R., McCarthy, L. A., Zhang, Q. F., Landes, C. F., Link, S., Nanophotonic Approaches for Chirality Sensing, 2021, *ACS Nano,* 15, 15538.
(6)Kim, R. M., Huh, J. H., Yoo, S., Kim, T. G., Kim, C., Kim, H., Han, J. H., Cho, N. H., Lim, Y. C., Im, S. W., Im, E., Jeong, J. R., Lee, M. H., Yoon, T. Y., Lee, H. Y., Park, Q. H., Lee, S., Nam, K. T., Enantioselective Sensing by Collective Circular Dichroism, 2022, *Nature,* 612, 470.
(7)Wei, X., Liu, J., Xia, G. J., Deng, J., Sun, P., Chruma, J. J., Wu, W., Yang, C., Wang, Y. G., Huang, Z., Enantioselective Photoinduced Cyclodimerization of a Prochiral Anthracene Derivative Adsorbed on Helical Metal Nanostructures, 2020, *Nat. Chem.,* 12, 551.
(8)Liu, J. J., Yang, L., Qin, P., Zhang, S. Q., Yung, K. K. L., Huang, Z. F., Recent Advances in Inorganic Chiral Nanomaterials, 2021, *Adv. Mater.,* 33, 2005506.
(9)Kuzyk, A., Schreiber, R., Fan, Z. Y., Pardatscher, G., Roller, E. M., Hogele, A., Simmel, F. C., Govorov, A. O., Liedl, T., DNA-Based Self-Assembly of Chiral Plasmonic Nanostructures with Tailored Optical Response, 2012, *Nature,* 483, 311.
(10)Shemer, G., Krichevski, O., Markovich, G., Molotsky, T., Lubitz, I., Kotlyar, A. B., Chirality of Silver Nanoparticles Synthesized on DNA, 2006, *J. Am. Chem. Soc.,* 128, 11006.
(11)Zhang, Q. F., Hernandez, T., Smith, K. W., Jebeli, S. A. H., Dai, A. X., Warning, L., Baiyasi, R., McCarthy, L. A., Guo, H., Chen, D. H., Dionne, J. A., Landes, C. F., Link, S., Unraveling the Origin of Chirality from Plasmonic Nanoparticle-Protein Complexes, 2019, *Science,* 365, 1475.
(12)George, J., Kar, S., Anupriya, E. S., Somasundaran, S. M., Das, A. D., Sissa, C., Painelli, A., Thomas, K. G., Chiral Plasmons: Au Nanoparticle Assemblies on Thermoresponsive Organic Templates, 2019, *ACS Nano,* 13, 4392.
(13)Lee, H. E., Ahn, H. Y., Mun, J., Lee, Y. Y., Kim, M., Cho, N. H., Chang, K., Kim, W. S., Rho, J., Nam, K. T., Amino-Acid- and Peptide-Directed Synthesis of Chiral Plasmonic Gold Nanoparticles, 2018, *Nature,* 556, 360.
(14)Gonzalez-Rubio, G., Mosquera, J., Kumar, V., Pedrazo-Tardajos, A., Llombart, P., Solis, D. M., Lobato, I., Noya, E. G., Guerrero-Martinez, A., Taboada, J. M., Obelleiro, F., MacDowell, L. G., Bals, S., Liz-Marzan, L. M., Micelle-Directed Chiral Seeded Growth on Anisotropic Gold Nanocrystals, 2020, *Science,* 368, 1472.
(15)Cho, N. H., Kim, Y. B., Lee, Y. Y., Im, S. W., Kim, R. M., Kim, J. W., Namgung, S. D., Lee, H. E., Kim, H., Han, J. H., Chung, H. W., Lee, Y. H., Han, J. W., Nam, K. T., Adenine Oligomer Directed Synthesis of Chiral Gold Nanoparticles, 2022, *Nat. Commun.,* 13, 3831.
(16)Ni, B., Mychinko, M., Gomez-Grana, S., Morales-Vidal, J., Obelleiro-Liz, M., Heyvaert, W., Vila-Liarte, D., Zhuo, X., Albrecht, W., Zheng, G., Gonzalez-Rubio, G., Taboada, J. M., Obelleiro, F., Lopez, N., Perez-Juste, J., Pastoriza-Santos, I., Colfen, H., Bals, S., Liz-Marzan, L. M., Chiral Seeded Growth of Gold Nanorods into Fourfold Twisted Nanoparticles with Plasmonic Optical Activity, 2023, *Adv. Mater.,* 35, 2208299.

(17)Ma, Yongjie, Cao, Zhaozhen, Hao, Jinjie, Zhou, Junhao, Yang, Zhijie, Yang, Yanzhao, Wei, Jingjing. Controlled Synthesis of Au Chiral Propellers from Seeded Growth of Au Nanoplates for Chiral Differentiation of Biomolecules, 2020, *J. Phys. Chem. C,* 124, 24306.
(18)Zhang, C. Q., Shoukat, C. A., Li, H. B., Ji, Y. L., Hu, Z. J., Wu, X. C., Cysteine-Mediated Etching of Gold Nanorods by Ferric Ions: Probing Cys Spatial Distribution Features on a Rod Surface, 2024, *J. Phys. Chem. C,* 128, 6672.
(19)Zhang, N. N., Shen, Z. L., Gao, S. Y., Peng, F., Cao, Z. J., Wang, Y., Wang, Z. Z., Zhang, W., Yang, Y., Liu, K., Sun, T. M., Synthesis and Plasmonic Chiroptical Properties of Double-Helical Gold Nanorod Enantiomers, 2023, *Adv. Opt. Mater.,* 11, 2203119.
(20)Chen, J. Q., Gao, X. S., Zheng, Q., Liu, J. B., Meng, D. J., Li, H. Y., Cai, R., Fan, H. Z., Ji, Y. L., Wu, X. C., Bottom-up Synthesis of Helical Plasmonic Nanorods and Their Application in Generating Circularly Polarized Luminescence, 2021, *ACS Nano,* 15, 15114.
(21)Horrer, A., Zhang, Y., Gerard, D., Beal, J., Kociak, M., Plain, J., Bachelot, R., Local Optical Chirality Induced by near-Field Mode Interference in Achiral Plasmonic Metamolecules, 2020, *Nano Lett.,* 20, 509.
(22)Srivastava, Sudhanshu, Santos, Aaron, Critchley, Kevin, Kim, Ki-Sub, Podsiadlo, Paul, Sun, Kai, Lee, Jaebeom, Xu, Chuanlai, Lilly, G. Daniel, Glotzer, Sharon C., Kotov, Nicholas A., Light-Controlled Self-Assembly of Semiconductor Nanoparticles into Twisted Ribbons, 2010, *Science,* 327, 1355.
(23)Yeom, Jihyeon, Yeom, Bongjun, Chan, Henry, Smith, Kyle W., Dominguez-Medina, Sergio, Bahng, Joong Hwan, Zhao, Gongpu, Chang, Wei-Shun, Chang, Sung-Jin, Chuvilin, Andrey, Melnikau, Dzmitry, Rogach, Andrey L., Zhang, Peijun, Link, Stephan, Král, Petr, Kotov, Nicholas A., Chiral Templating of Self-Assembling Nanostructures by Circularly Polarized Light, 2015, *Nat. Mater.,* 14, 66.
(24)Kim, J. Y., Yeom, J., Zhao, G., Calcaterra, H., Munn, J., Zhang, P., Kotov, N., Assembly of Gold Nanoparticles into Chiral Superstructures Driven by Circularly Polarized Light, 2019, *J. Am. Chem. Soc.,* 141, 11739.
(25)Morisawa, K., Ishida, T., Tatsuma, T., Photoinduced Chirality Switching of Metal-Inorganic Plasmonic Nanostructures, 2020, *ACS Nano,* 14, 3603.
(26)Saito, K., Tatsuma, T., Chiral Plasmonic Nanostructures Fabricated by Circularly Polarized Light, 2018, *Nano Lett.,* 18, 3209.
(27)Qiao, T., Bordoloi, P., Miyashita, T., Dionne, J. A., Tang, M. L., Tuning the Chiral Growth of Plasmonic Bipyramids Via the Wavelength and Polarization of Light, 2024, *Nano Lett.,* 24, 2611.
(28)Lee, S. H., Fan, C. H., Movsesyan, A., Bürger, J., Wendisch, F. J., Menezes, L. D., Maier, S. A., Ren, H. R., Liedl, T., Besteiro, L. V., Govorov, A. O., Cortés, E., Unraveling the Chirality Transfer from Circularly Polarized Light to Single Plasmonic Nanoparticles, 2024, *Angew. Chem. Int. Ed.,* 63, e202319920.
(29)Ishida, T., Isawa, A., Kuroki, S., Kameoka, Y., Tatsuma, T., All-Plasmonic-Metal Chiral Nanostructures Fabricated by Circularly Polarized Light, 2023, *Appl. Phys. Lett.,* 123, 061111.
(30)Avalos-Ovando, O., Lorca, V. B., Besteiro, L. V., Movsesyan, A., Wang, Z. M., Markovich, G., Govorov, A. O., Universal Imprinting of Chirality with Chiral Light by Employing Plasmonic Metastructures, 2023, *Appl. Phys. Rev.,* 10, 031412.
(31)Besteiro, L. V., Movsesyan, A., Avalos-Ovando, O., Lee, S., Cortes, E., Correa-Duarte, M. A., Wang, Z. M., Govorov, A. O., Local Growth Mediated by Plasmonic Hot Carriers: Chirality from Achiral Nanocrystals Using Circularly Polarized Light, 2021, *Nano Lett.,* 21, 10315.
(32)Movsesyan, Artur, Muravitskaya, Alina, Besteiro, Lucas V., Santiago, Eva Yazmin, Ávalos‐Ovando, Oscar, Correa‐Duarte, Miguel A., Wang, Zhiming, Markovich, Gil,

Govorov, Alexander O., Creating Chiral Plasmonic Nanostructures Using Chiral Light in a Solution and on a Substrate: The near‐Field and Hot‐Electron Routes, 2023, *Adv. Opt. Mater.,* 11, 2300013.
(33)Sun, Y. G., Xia, Y. N., Triangular Nanoplates of Silver: Synthesis, Characterization, and Use as Sacrificial Templates for Generating Triangular Nanorings of Gold, 2003, *Adv. Mater.,* 15, 695.
(34)Callegari, A., Tonti, D., Chergui, M., Photochemically Grown Silver Nanoparticles with Wavelength-Controlled Size and Shape, 2003, *Nano Lett.,* 3, 1565.
(35)Jin, R. C., Cao, Y. C., Hao, E. C., Metraux, G. S., Schatz, G. C., Mirkin, C. A., Controlling Anisotropic Nanoparticle Growth through Plasmon Excitation, 2003, *Nature,* 425, 487.
(36)Jin, R. C., Cao, Y. W., Mirkin, C. A., Kelly, K. L., Schatz, G. C., Zheng, J. G., Photoinduced Conversion of Silver Nanospheres to Nanoprisms, 2001, *Science,* 294, 1901.
(37)Langille, M. R., Personick, M. L., Mirkin, C. A., Plasmon-Mediated Syntheses of Metallic Nanostructures, 2013, *Angew. Chem. Int. Ed.,* 52, 13910.
(38)Maillard, M., Huang, P. R., Brus, L., Silver Nanodisk Growth by Surface Plasmon Enhanced Photoreduction of Adsorbed [Ag^+], 2003, *Nano Lett.,* 3, 1611.
(39)Redmond, P. L., Wu, X. M., Brus, L., Photovoltage and Photocatalyzed Growth in Citrate-Stabilized Colloidal Silver Nanocrystals, 2007, *J. Phys. Chem. C,* 111, 8942.
(40)Wu, X. M., Redmond, P. L., Liu, H. T., Chen, Y. H., Steigerwald, M., Brus, L., Photovoltage Mechanism for Room Light Conversion of Citrate Stabilized Silver Nanocrystal Seeds to Large Nanoprisms, 2008, *J. Am. Chem. Soc.,* 130, 9500.
(41)Golze, S. D., Hughes, R. A., Rouvimov, S., Neal, R. D., Demille, T. B., Neretina, S., Plasmon-Mediated Synthesis of Periodic Arrays of Gold Nanoplates Using Substrate-Immobilized Seeds Lined with Planar Defects, 2019, *Nano Lett.,* 19, 5653.
(42)Zhai, Y., DuChene, J. S., Wang, Y. C., Qiu, J., Johnston-Peck, A. C., You, B., Guo, W., DiCiaccio, B., Qian, K., Zhao, E. W., Ooi, F., Hu, D., Su, D., Stach, E. A., Zhu, Z., Wei, W. D., Polyvinylpyrrolidone-Induced Anisotropic Growth of Gold Nanoprisms in Plasmon-Driven Synthesis, 2016, *Nat. Mater.,* 15, 889.
(43)Guo, W., Johnston-Peck, A. C., Zhang, Y., Hu, Y., Huang, J., Wei, W. D., Cooperation of Hot Holes and Surface Adsorbates in Plasmon-Driven Anisotropic Growth of Gold Nanostars, 2020, *J. Am. Chem. Soc.,* 142, 10921.
(44)Xue, C., Metraux, G. S., Millstone, J. E., Mirkin, C. A., Mechanistic Study of Photomediated Triangular Silver Nanoprism Growth, 2008, *J. Am. Chem. Soc.,* 130, 8337.
(45)Golze, S. D., Porcu, S., Zhu, C., Sutter, E., Ricci, P. C., Kinzel, E. C., Hughes, R. A., Neretina, S., Sequential Symmetry-Breaking Events as a Synthetic Pathway for Chiral Gold Nanostructures with Spiral Geometries, 2021, *Nano Lett.,* 21, 2919.
(46)Zhang, J., Li, S. Z., Wu, J. S., Schatz, G. C., Mirkin, C. A., Plasmon-Mediated Synthesis of Silver Triangular Bipyramids, 2009, *Angew. Chem. Int. Ed.,* 48, 7787.
(47)Dombi, P., Horl, A., Racz, P., Marton, I., Trugler, A., Krenn, J. R., Hohenester, U., Ultrafast Strong-Field Photoemission from Plasmonic Nanoparticles, 2013, *Nano Lett.,* 13, 674.
(48)Brongersma, M. L., Halas, N. J., Nordlander, P., Plasmon-Induced Hot Carrier Science and Technology, 2015, *Nat. Nanotechnol.,* 10, 25.
(49)Brown, A. M., Sundararaman, R., Narang, P., Goddard, W. A., 3rd, Atwater, H. A., Nonradiative Plasmon Decay and Hot Carrier Dynamics: Effects of Phonons, Surfaces, and Geometry, 2016, *ACS Nano,* 10, 957.
(50)Cortes, E., Xie, W., Cambiasso, J., Jermyn, A. S., Sundararaman, R., Narang, P., Schlucker, S., Maier, S. A., Plasmonic Hot Electron Transport Drives Nano-Localized Chemistry, 2017, *Nat. Commun.,* 8, 14880.

(51)Hobbs, R. G., Putnam, W. P., Fallahi, A., Yang, Y., Kartner, F. X., Berggren, K. K., Mapping Photoemission and Hot-Electron Emission from Plasmonic Nanoantennas, 2017, *Nano Lett.,* 17, 6069.
(52)Jermyn, Adam S., Tagliabue, Giulia, Atwater, Harry A., Goddard, William A., Narang, Prineha, Sundararaman, Ravishankar. Transport of Hot Carriers in Plasmonic Nanostructures, 2019, *Phys. Rev. Mater.,* 3, 075201.
(53)Gargiulo, J., Berté, R., Li, Y., Maier, S. A., Cortés, E., From Optical to Chemical Hot Spots in Plasmonics, 2019, *Acc. Chem. Res.,* 52, 2525.
(54)Zhan, C., Yi, J., Hu, S., Zhang, X. G., Wu, D. Y., Tian, Z. Q., Plasmon-Mediated Chemical Reactions, 2023, *Nat. Rev. Methods Primers,* 3, 12.
(55)Ogata, R., Nishi, H., Ishida, T., Tatsuma, T., Visualization of Nano-Localized and Delocalized Oxidation Sites for Plasmon-Induced Charge Separation, 2021, *Nanoscale,* 13, 681.
(56)Haynes, William M, 2012, The Crc Handbook of Chemistry and Physics 93rd Edition, CRC Press Boca Raton.
(57)Saito, K., Nemoto, Y., Ishikawa, Y., Circularly Polarized Light-Induced Chiral Growth of Achiral Plasmonic Nanoparticles Dispersed in a Solution, 2024, *Nano Lett.,* 24, 12840.
(58)Ghalawat, M., Feferman, D., Besteiro, L. V., He, W. T., Movsesyan, A., Muravitskaya, A., Valdez, J., Moores, A., Wang, Z. M., Ma, D. L., Govorov, A. O., Markovich, G., Chiral Symmetry Breaking in Colloidal Metal Nanoparticle Solutions by Circularly Polarized Light, 2024, *ACS Nano,* 18, 28279.
(59)Li, Qian, Zhuo, Xiaolu, Li, Shuang, Ruan, Qifeng, Xu, Qing-Hua, Wang, Jianfang. Production of Monodisperse Gold Nanobipyramids with Number Percentages Approaching 100% and Evaluation of Their Plasmonic Properties, 2015, *Adv. Opt. Mater.,* 3, 801.
(60)Zhuo, X. L., Zhu, X. Z., Li, Q., Yang, Z., Wang, J. F., Gold Nanobipyramid-Directed Growth of Length-Variable Silver Nanorods with Multipolar Plasmon Resonances, 2015, *ACS Nano,* 9, 7523.
(61)Sanchez-Iglesias, A., Winckelmans, N., Altantzis, T., Bals, S., Grzelczak, M., Liz-Marzan, L. M., High-Yield Seeded Growth of Monodisperse Pentatwinned Gold Nanoparticles through Thermally Induced Seed Twinning, 2017, *J. Am. Chem. Soc.,* 139, 107.
(62)Thrall, E. S., Steinberg, A. P., Wu, X. M., Brus, L. E., The Role of Photon Energy and Semiconductor Substrate in the Plasmon-Mediated Photooxidation of Citrate by Silver Nanoparticles, 2013, *J. Phys. Chem. C,* 117, 26238.
(63)Zu, S., Han, T. Y., Jiang, M. L., Lin, F., Zhu, X., Fang, Z. Y., Deep-Subwavelength Resolving and Manipulating of Hidden Chirality in Achiral Nanostructures, 2018, *ACS Nano,* 12, 3908.
(64)Oshikiri, T., Sun, Q., Yamada, H., Zu, S., Sasaki, K., Misawa, H., Extrinsic Chirality by Interference between Two Plasmonic Modes on an Achiral Rectangular Nanostructure, 2021, *ACS Nano,* 15, 16802.
(65)Li, N. N., Yin, H., Zhuo, X. L., Yang, B. C., Zhu, X. M., Wang, J. F., Infrared-Responsive Colloidal Silver Nanorods for Surface-Enhanced Infrared Absorption, 2018, *Adv. Opt. Mater.,* 6, 1800436.
(66)Li, Q., Jiang, R. B., Ming, T., Fang, C. H., Wang, J. F., Crystalline Structure-Dependent Growth of Bimetallic Nanostructures, 2012, *Nanoscale,* 4, 7070.
(67)Sánchez-Iglesias, A., Zhuo, X. L., Albrecht, W., Bals, S., Liz-Marzán, L. M., Tuning Size and Seed Position in Small Silver Nanorods, 2020, *ACS Mater. Lett.,* 2, 1246.
(68)Pietrobon, B., McEachran, M., Kitaev, V., Synthesis of Size-Controlled Faceted Pentagonal Silver Nanorrods with Tunable Plasmonic Properties and Self-Assembly of These Nanorods, 2009, *ACS Nano,* 3, 21.

(69)Gómez-Graña, S., Goris, B., Altantzis, T., Fernández-López, C., Carbó-Argibay, E., Guerrero-Martínez, A., Almora-Barrios, N., López, N., Pastoriza-Santos, I., Pérez-Juste, J., Bals, S., Van Tendeloo, G., Liz-Marzán, L. M., Au@Ag Nanoparticles: Halides Stabilize {100} Facets, 2013, *J. Phys. Chem. Lett.,* 4, 2209.
(70)Duan, Y. C., Rani, S., Newberg, J. T., Teplyakov, A. V., Investigation of the Influence of Oxygen Plasma on Supported Silver Nanoparticles, 2018, *J. Vac. Sci. Technol. A.,* 36, 01B101.
(71)Gehl, B., Frömsdorf, A., Aleksandrovic, V., Schmidt, T., Pretorius, A., Flege, J. I., Bernstorff, S., Rosenauer, A., Falta, J., Weller, H., Bäumer, M., Structural and Chemical Effects of Plasma Treatment on Close-Packed Colloidal Nanoparticle Layers, 2008, *Adv. Funct. Mater.,* 18, 2398.
(72)Movsesyan, A., Santiago, E. Y., Burger, S., Correa-Duarte, M. A., Besteiro, L., Wang, Z. M., Govorov, A. O., Plasmonic Nanocrystals with Complex Shapes for Photocatalysis and Growth: Contrasting Anisotropic Hot-Electron Generation with the Photothermal Effect, 2022, *Adv. Opt. Mater.,* 10, 2102663.
(73)Christensen, N. E., The Band Structure of Silver and Optical Interband Transitions, 1972, *Physica Status Solidi (B),* 54, 551.
(74)Kamarudheen, R., Aalbers, G. J. W., Hamans, R. F., Kamp, L. P. J., Baldi, A., Distinguishing among All Possible Activation Mechanisms of a Plasmon-Driven Chemical Reaction, 2020, *ACS Energy Lett.,* 5, 2605.
(75)Al-Zubeidi, A., Wang, Y., Lin, J., Flatebo, C., Landes, C. F., Ren, H., Link, S., D-Band Holes React at the Tips of Gold Nanorods, 2023, *J. Phys. Chem. Lett.,* 14, 5297.
(76)Muravitskaya, A., Movsesyan, A., Avalos-Ovando, O., Lorca, V. A. B., Correa-Duarte, M. A., Besteiro, L. V., Liedl, T., Yu, P., Wang, Z. M., Markovich, G., Govorov, A. O., Hot Electrons and Electromagnetic Effects in the Broadband Au, Ag, and Ag-Au Nanocrystals: The Uv, Visible, and Nir Plasmons, 2023, *ACS Photonics,* 11, 68.
(77)Baffou, G., Quidant, R., de Abajo, F. J. G., Nanoscale Control of Optical Heating in Complex Plasmonic Systems, 2010, *ACS Nano,* 4, 709.
(78)Baffou, G., Quidant, R., Girard, C., Thermoplasmonics Modeling: A Green's Function Approach, 2010, *Phys. Rev. B,* 82, 165424.
(79)Kliger, David S, Lewis, James W, 2012, Polarized Light in Optics and Spectroscopy, Elsevier. 0080571042.
(80)Jensen, HP, Schellman, JA, Troxell, T. Modulation Techniques in Polarization Spectroscopy, 1978, *Appl. Spectrosc.,* 32, 192.
(81)Yao, Yuan, Ugras, Thomas J., Meyer, Talisi, Dykes, Matthew, Wang, Da, Arbe, Arantxa, Bals, Sara, Kahr, Bart, Robinson, Richard D., Extracting Pure Circular Dichroism from Hierarchically Structured Cds Magic Cluster Films, 2022, *ACS Nano,* 16, 20457.
(82)Braslavsky, S. E., Glossary of Terms Used in Photochemistry 3(Rd) Edition (Iupac Recommendations 2006), 2007, *Pure Appl. Chem.,* 79, 293.

Supporting Information

Supporting Information is available from the Wiley Online Library or from the author.

Surface ligands increased the spatial selectivity of silver deposition on achiral silver nanorods under circularly polarized light, leading to nanostructures with enhanced structural chirality. With a *g-factor* ~ of 0.05, the optical dissymmetry of these chiral nanostructures is one order of magnitude larger than those grown from achiral silver nanorods without surface ligands engineering.

Increasing the Structural Chirality of Metal Nanocrystals Created by Circularly Polarized Light via Surface Ligand Engineering

TOC figure